AGU Advances

RESEARCH ARTICLE
10.1029/2020AV000180

Key Points:
- We used a new dynamic LUE model to estimate global GPP for 1982–2016
- Increasing GPP in northern high latitudes is offset by GPP decline in the tropics
- Global GPP is shifting from being temperature limited to VPD limited

Supporting Information:
- Supporting Information S1
- Original Version of Manuscript
- Peer Review History
- First Revision of Manuscript
- Second Revision of Manuscript
- Third Revision of Manuscript
- Fourth Revision of Manuscript [Accepted]
- Authors' Response to Peer Review Comments

Correspondence to:
N. Madani,
nima.madani@jpl.nasa.gov

Citation:
Madani, N., Parazoo, N. C., Kimball, J. S., Ballantyne, A. P., Reichle, R. H., Maneta, M., et al. (2020). Recent amplified global gross primary productivity due to temperature increase is offset by reduced productivity due to water constraints. *AGU Advances*, *2*, e2020AV000180. https://doi.org/10.1029/2020AV000180

Received 5 MAR 2020
Accepted 21 OCT 2020

The peer review history for this article is available as a PDF in the Supporting Information.

Recent Amplified Global Gross Primary Productivity Due to Temperature Increase Is Offset by Reduced Productivity Due to Water Constraints

Nima Madani[1], Nicholas C. Parazoo[1], John S. Kimball[2,3], Ashley P. Ballantyne[2], Rolf H. Reichle[4], Marco Maneta[5], Sassan Saatchi[1], Paul I. Palmer[6,1], Zhihua Liu[2,3], and Torbern Tagesson[7]

[1]Jet Propulsion Laboratory, California Institute of Technology, Pasadena, CA, USA, [2]Numerical Terradynamic Simulation Group, W.A. Franke College of Forestry and Conservation, University of Montana, Missoula, MT, USA, [3]Department of Ecosystem and Conservation Sciences, W.A. Franke College of Forestry and Conservation, University of Montana, Missoula, Montana, USA, [4]Global Modeling and Assimilation Office, NASA Goddard Space Flight Center, Greenbelt, MD, USA, [5]Department of Geosciences, University of Montana, Missoula, MT, USA, [6]National Centre for Earth Observation, School of GeoSciences, University of Edinburgh, Edinburgh, UK, [7]Department of Physical Geography and Ecosystem Science, Lund University, Lund, Sweden

Abstract Satellite remote sensing observations show an increased greenness trend over land in recent decades. While greenness observations can indicate increased productivity, estimation of total annual productivity is highly dependent on vegetation response to climate and environmental conditions. Models have been struggling to determine how much carbon is taken up by plants as a result of increased atmospheric CO_2 fertilization. Current remote sensing light use efficiency (LUE) models contain considerable uncertainty due to the lack of spatial and temporal variability in maximum LUE parameter and climate sensitivity defined for global plant functional types (PFTs). We used the optimum LUE (LUE_{opt}) previously derived from the global FLUXNET network to improve estimation of global gross primary productivity (GPP) for the period 1982–2016. Our results indicate increasing GPP in northern latitudes owing to reduced cold temperature constraints on plant growth, thereby suggesting increasing negative carbon-climate feedback in high latitudes. In the tropics, by contrast, our results indicate an emerging positive climate feedback, mainly due to increasing atmospheric vapor pressure deficit (VPD). Further pervasive VPD increase is likely to continue to reduce global GPP and amplify carbon emissions.

Plain Language Summary In light use efficiency (LUE) models, plant production is linearly related to canopy absorbed photosynthetically active radiation (APAR), based on the assumption that plants absorb and convert solar radiant energy into vegetation biomass with a given efficiency rate. Here, we used an enhanced LUE model driven with remote sensing observations to estimate plant productivity for 1982–2016. We found that over the study period, plant photosynthetic activity has increased over northern latitudes, which may partially offset the CO_2 emissions from fossil fuel consumption. However, our results show that productivity in the tropical zones is declining rapidly due to increased water stress. With increased warming, water limitations are expected to increasingly limit global plant productivity.

1. Introduction

Life on Earth is supported by plant photosynthesis through gross primary productivity (GPP), which represents the largest annual carbon flux linked directly linked to environmental conditions and atmospheric CO_2 concentrations (Beer et al., 2010). Human reliance on plant photosynthesis includes GPP allocation to food, fiber, and fuel production, as well as ecosystem services provided by offsetting atmospheric CO_2 emissions from fossil fuel consumption (Norby et al., 2010; Quéré et al., 2018; Schimel et al., 2015). For the past three decades, global satellite remote sensing has provided direct observations of the amount of photosynthetic leaf area (Myneni et al., 2002). These observations serve as primary inputs for satellite-driven diagnostic models of GPP such as light use efficiency (LUE) models (Running et al., 2004). Satellite observations from the Advanced Very High Resolution Radiometer (AVHRR) and the MODerate resolution Image Spectrometer (MODIS) sensors provide consistent global measurements of changes in photosynthetic leaf

area starting in June 1981 (Zhu et al., 2013). During this period, the global mean atmospheric CO_2 concentration has increased by 20%, from 340 ppm in 1981 to 407 ppm in 2016 (Etheridge et al., 1996; Keeling et al., 2005). This increase has coincided with widespread increase in leaf area (Zhu et al., 2016) and changes in vegetation phenology, including earlier spring green-up (Cleland et al., 2007; Cong et al., 2013; Zhu et al., 2016). Conversely, anomalous changes in global productivity associated with climate extremes driven by the El Niño–Southern Oscillation (ENSO) have also been observed and modeled (Liu et al., 2017; Nemani et al., 2003; Zhao & Running, 2010; Zhu et al., 2018). In addition to ENSO, other factors coinciding with water scarcity, high temperatures, and large fires (Reichstein et al., 2013) have significantly impacted the global carbon cycle over the past few decades. Some of these satellite-observed events, including large-scale wind throw, biotic events, pest outbreaks, and deforestation, have significantly impacted global vegetation cover (Reichstein et al., 2013; Zscheischler et al., 2013, 2014). Extreme events associated with cold temperature events and heavy rain are also known to impact the global carbon cycle (Zscheischler et al., 2014). However, the current generation of remote sensing driven LUE models has several key limitations that make it difficult to properly estimate long-term GPP trends.

The biome property lookup table approach is a well-known shortcoming of LUE models (Madani et al., 2014; Turner et al., 2002; Wang et al., 2010; Way et al., 2005). In this approach, photosynthetic rate is constrained by biome-specific, predefined thresholds to represent optimum climatic conditions for plant productivity. In addition, the maximum LUE rate, which defines potential GPP, is typically assumed to be temporally constant (e.g., Kimball et al., 2017; Running et al., 2004). Improving these basic GPP model limitations will reduce uncertainty in global GPP estimates and advance the understanding of the terrestrial biosphere response to environmental change and climate extremes.

The variability in CO_2 sources and sinks in natural environments including ocean and land ecosystems is driven by the variability in atmospheric CO_2 accumulation rate (Keenan et al., 2016). However, estimation of the carbon sources and sinks in land ecosystems remains challenging, where the range of variability in estimated annual GPP and its interannual variability and trend is large among Earth system, LUE, and machine learning-based models (Anav et al., 2015). Even though all of the global models reviewed by Anav et al. (2015) show positive annual GPP trends over the last few decades, there are large discrepancies in the estimated magnitude of GPP trends and interannual variability. Previous studies noted that global ecosystem net primary productivity models that use a satellite data-driven LUE modeling approach show an increasing trend for the period 1982–1999 (Nemani et al., 2003), but this productivity trend diverged after 2000 due to climatic changes, including severe droughts (Zhao & Running, 2010).

Here, we provide a quantitative and mechanistic multidecadal assessment of global GPP trends and anomalies using an enhanced remote sensing LUE model. Our primary goal is to identify the most important factors driving long-term GPP change across key bioclimatic regions. We model global monthly GPP using the third-generation Global Inventory Modeling and Mapping Studies (GIMMS3g) fraction of photosynthetically active radiation (FPAR) record for the period 1982–2016 (Zhu et al., 2013) as a primary model input. By building upon our previous experience (Madani et al., 2014; Madani, Kimball, Jones, et al., 2017; Madani, Kimball, & Running, 2017), our enhanced LUE model provides temporally and spatially explicit dynamic optimum LUE (LUE_{opt}) information that supports improved estimates of long-term (1982–2016) GPP trends across the globe.

2. Methods

2.1. Geospatial Data

We acquired the global semimonthly GIMMS3g FPAR data (Zhu et al., 2013) for the 35-year (1982–2016) study period. GIMMS3g FPAR is created based on the relationship between the new improved GIMMS3g normalized difference vegetation index (NDVI) and best quality MODIS leaf area index (LAI) and FPAR products for the overlapping period 2000–2009 using a neural network algorithm (Zhu et al., 2013). We obtained meteorological and other geospatial information, including monthly minimum air temperature, dew point temperature, incoming shortwave solar radiation, and surface-to-root-zone soil moisture (SM) from the Modern-Era Retrospective analysis for Research and Applications, Version 2 (MERRA-2; Gelaro et al., 2017). We aggregated FPAR semimonthly data to monthly scales by averaging the FPAR values over each month and resampled the MERRA-2 ½° latitude by 5/8° longitude spatial resolution meteorological data using

nearest neighboring approach to match the FPAR 0.08° spatial resolution for modeling GPP at monthly time scale for the entire GIMMS3g record. Adopting the finer FPAR resolution for the GPP model simulations, rather than the coarser resolution of the meteorological data, allowed us to better capture the effect of land cover and land use change on GPP (Robinson et al., 2018).

2.2. Spatially Explicit LUE_{opt} Data

Global, spatially distributed LUE_{opt} values were derived from the flux tower-based estimates of LUE_{opt} (Madani, Kimball, & Running, 2017). The tower eddy covariance CO_2 flux measurement sites presented in Madani, Kimball, and Running (2017) represent a broad range of global biomes (Table S1 in the supporting information) with at least 2 years of daily ecosystem CO_2 exchange measurement records at each site. In this approach, the upper 98–99.5% bin of FLUXNET tower daily gap-filled GPP values for each tower site is selected to represent the maximum daily GPP (GPP_{max}). It is assumed that in the upper bin of GPP, plant productivity is not restricted by climate constraint factors (Kergoat et al., 2008; Madani et al., 2014). The FPAR data collocated with FLUXNET tower site locations are temporally matched with the tower GPP records, and PAR is resampled to FPAR resolution using nearest neighboring approach. For each tower site, LUE is defined as follows:

$$LUE = \frac{GPP_{max}}{\mathrm{APAR}} \tag{1}$$

In Equation 1, APAR is the absorbed photosynthetically active radiation (PAR), which is derived from the product of FPAR defined from the GIMMS3g record and the daily PAR, estimated as half of the global incoming shortwave solar radiation derived from the MERRA-2 global reanalysis (Gelaro et al., 2017). For each of the tower sites the averaged daily LUE observations from Equation 1 are used to represent the LUE_{opt} value of that specific site.

We extrapolated the tower-based LUE_{opt} values to the global domain based on a generalized additive model (GAM) framework (Hastie & Tibshirani, 1990). The model used several explanatory variables for LUE_{opt} including average annual long-term temperature from MERRA-2 to determine climate sensitivity, the satellite observed solar-induced chlorophyll fluorescence (SIF) from the Global Ozone Monitoring Experiment-2 (GOME-2) (Köhler et al., 2015) to represent biome heterogeneity in productivity within the land cover classifications defined by MODIS MOD12-type-2 (Friedl et al., 2010) classes, maximum and minimum annual FPAR to represent annual changes in land cover as well as the potential effect of the atmospheric CO_2 concentration growth rate on plant leaf area (Zhu et al., 2016). We used the GAM model to provide annual LUE_{opt} information distributed over the global vegetated land areas from 1982–2016 at 8-km spatial resolution. (Refer to Table S2 for the parametric and smoothed coefficient functions of selected environmental predictors used to extrapolate tower estimated LUE_{opt}). Our model was trained on measurements from a subset of global tower sites from the La Thuile FLUXNET synthesis data set (Baldocchi, 2008) and was tested using independent tower sites from the 2015 FLUXNET record (Pastorello et al., 2020; Refer to Figure S1 for location of tower sites). The trained model was then used along with dynamic annual FPAR observations to generate corresponding spatially explicit LUE_{opt} data from 1982–2016.

2.3. Modeling Global GPP

The LUE model used here is similar to the National Aeronautics and Space Administration (NASA) Soil Moisture Active Passive (SMAP) mission's level 4 carbon model algorithm (L4C) (Jones et al., 2017), which uses SM as a water supply constraint factor, enabling improved GPP accuracy in water limited regions (Jones et al., 2017; Kimball et al., 2012; Stocker et al., 2019). Our model also accounts for changes in atmospheric vapor pressure deficit (VPD), which we modeled following Murray (1967):

$$VPD = 611 \times e^{\frac{17.502 \times Ta}{Ta + 240.97}} - 611 \times e^{\frac{17.502 \times Td}{Td + 240.97}} \tag{1}$$

where T_a is the average daily temperature in degrees Celsius and T_d is the dew point obtained from MERRA2.

Our LUE model provides enhanced GPP estimates (hereinafter termed GPP_{Enh}) as follows:

$$GPP_{Enh} = FPAR \times PAR \times LUE_{opt} \times fVPD \times fSM \times fT_{min} \quad (2)$$

where $fVPD$, fSM, and fT_{min} represent dimensionless environmental constraint functions ranging from 0 (fully constrained) to 1 (no effect) that describe reductions from optimal GPP due to water and temperature stress:

$$fT = \begin{cases} 0, & T_{min} \le T_{Mmin} \\ \dfrac{T_{min} - T_{Mmin}}{T_{Mmax} - T_{Mmin}}, & T_{Mmin} < T_{min} < T_{Mmax} \\ 1, & T_{min} \ge T_{Mmax}. \end{cases} \quad (3)$$

$$fVPD = \begin{cases} 0, \ VPD \ge VPD_{Max} \\ 1 - \dfrac{VPD - VPD_{Min}}{VPD_{Max} - VPD_{Min}}, \ VPD_{Min} < VPD < VPD_{Max} \\ 1, \ VPD \le VPD_{Min}. \end{cases} \quad (4)$$

The Min and Max subscripts in Equations 4 and 5 represent the minimum and maximum defined thresholds for minimum daily air temperature (T_{min}) and VPD functions derived from the bioclimatic factors controlling productivity at global scales (Madani, Kimball, & Running, 2017), in addition to ecosystems phenological patterns indicated from flux tower observations. In this regard, we used global tower sites to acquire minimum and maximum thresholds for the T_{min} and VPD bio-climatic variables. T_{min} in the LUE model defines the length of plant activity. We defined T_{Mmin} and T_{Mmax} as 10 and 20 quantiles of the daily GPP climatology and recorded SIF value of the corresponding time for a given tower location. We used a similar technique to establish the VPD thresholds with the exception of using the upper 90 daily GPP quantiles to assess the negative impact of high VPD on stomatal conductance. We then used the observed SIF seasonality to generate spatial maps of environmental constraint factors and used the constraint factors only for regions where seasonality in productivity, confirmed by SIF observations, was shown to be controlled by the specific constraint factor (Madani, Kimball, & Running, 2017).

Daily SM for the global simulations was normalized as a daily proportion of the maximum and minimum reported local SM values from the long-term (1982–2016) record for each pixel. The resulting normalized SM values were aggregated to monthly time steps and used in the following nonlinear constraint function built upon a nonlinear relationship between SM and LUE (Stocker et al., 2018) to estimate GPP in Equation 2:

$$fSM = 1 - (SM - 1)^2 \quad (5)$$

2.4. Validation and Analysis

We validated GPP_{Enh} against flux tower GPP observations for the 2007 to 2014 period obtained from the 2015 FLUXNET record, where the tower validation sites were independent from the sites used for model training (Figure S1). The tower sites used for model training and validation were selected on the basis of being representative of the major global biomes and having at least 2 years of CO_2 flux measurements. To assess different factors contributing to changes in GPP, we executed the GPP_{Enh} model on a monthly basis with static APAR (APAR climatology) and variable climatic factors ($fVPD \times fSM \times fT_{min}$) and once again with static climatic factors (climatology of $fVPD \times fSM \times fT_{min}$) and dynamic APAR data. We extended our analysis by detrending GPP and underlying factors controlling productivity, including annual FPAR, SM, PAR, T_{min}, and VPD, and performed annual and multidecadal assessment of GPP anomalies at regional and global scales. We calculated the anomalies in time series data by removing the linear trend. In this regard, residuals e_t, or the differences between the data values (y) and the corresponding linearly fitted values over time x_t , are defined as follows:

$$e_t = y_t - \beta_0 - \beta_1 x_{1,t} - \beta_2 x_{2,t} - ....\beta_k x_{k,t} \quad (6)$$

For comparison, we used the GIMMS FPAR data and MERRA-2 meteorology to model GPP using fixed LUE_{max} values used by the MODIS MOD17 operational (Collection 6) GPP product (Zhao &

Running, 2010). We also compared our GPP_{Enh} key findings with the TRENDY ensemble mean GPP, atmospheric CO_2 inversion model results, and SIF observations.

We used the ensemble mean GPP of 10 dynamic global vegetation models (DGVMs; Table S3) from the TRENDY-v7 project (Quéré et al., 2018; Sitch et al., 2015) for comparison with our GPP model results. The selected models with spatial resolutions of 0.5° to 2° for the period 1982–2016 use climate, land use, and CO_2 forcing effects on ecosystem productivity. We also acquired net biome productivity (NBP) data from CO_2 inversion model results with 1° monthly spatiotemporal resolution from six inversion models, including CT2017, CTE2018, CarboScope s76_v4.2, CarboScope s85_v4.2, JAMSTEC, and CAMS (see Table S4 for references and details) to compare with our LUE model findings. In addition to modeled ecosystem productivity data, we used SIF from the scanning imaging absorption spectrometer for atmospheric chartography (SCIAMACHY) for 2003–2011 (Joiner et al., 2012) and GOME-2 (Köhler et al., 2015) for 2007–2016 as remote sensing indicators of ecosystem productivity. To mitigate artifacts in the GOME-2 SIF retrievals after mid-2012 due to sensor degradation (Zhang et al., 2018), we corrected the drift in time series data by matching the mean of observations after mid-2012 to the mean values from 2007 to mid-2012. We generated the anomalies in annual GPP_{Enh}, NBP, TRENDY GPP, and SIF by calculating the departure from long-term average and normalized the values using:

$$z_i = 2 \times \frac{x_i - min(x)}{max(x) - min(x)} - 1 \tag{7}$$

where $x = (x_1, ...x_n)$ and z_i denotes i^{th} normalized data. We compared these data over tropical and northern high latitudes, the two highly important regions for carbon cycle dynamics.

3. Results

The new GPP_{Enh} model explains 80% of the variation in annual GPP across flux tower sites, with an RMSE of 331 g C m^{-2} $year^{-1}$. The variance explained declines to 75%, and RMSE increases to 506 g C m^{-2} $year^{-1}$ for the model with constant LUE_{max} (and otherwise the same meteorology and FPAR data; Figure S2; Refer to Figure S3 for comparison between GPP_{Enh} with the conventional LUE model over independent test sites). The improvement in the GPP estimate was a result of the environmental explanatory variables that explained ~56% of the spatial variation ($p < 0.0001$) among tower observed LUE_{opt} values. However, the fixed LUE_{max} parameters defined for each land cover type could only explain ~36% of the variance in tower observed LUE_{opt}.

The 35-year linear trends in GPP demonstrate that, in ~50% of the vegetated land areas, GPP is increasing by up to 20 g C m^{-2} $year^{-1}$, whereas the GPP of tropical regions is declining at the same rate. Black dots represent pixels with statistically significant trends ($p < 0.05$).

Our estimated global average GPP over the last three decades is 130 ± 1.6 Pg $year^{-1}$. The lowest GPP is estimated for 1983 (126 Pg $year^{-1}$), and the highest GPP is for 2011 (133 Pg $year^{-1}$). Over the study period, annual GPP trends indicate that GPP in Amazonia and the Southeast Asian tropics decreased at rates of up to 20 g C m^{-2} $year^{-1}$ (at grid scale), while GPP in the northern latitudes increased at the same rate (Figure 1). To further assess the regional GPP trends, we performed a multidecadal GPP assessment for selected latitudinal zones.

In the northern high latitudes (>45°N) GPP began to increase by 0.07 Pg $year^{-1}$ from 1982 onward, which represents about 0.4% increase in GPP per year relative to the 35-year mean (17.9 Pg C). In contrast, equatorial GPP (10°S to 10°N) has steadily declined since the 1980s, leading to a reduction of 0.5–1 Pg over 35 years compared to the long-term average (Figure 2).

We further analyzed the main factors affecting global annual GPP anomalies. VPD contributes the highest variability to GPP in tropical regions. In arid environments, water restrictions defined by SM and VPD are the primary limiting factors. In the northern latitudes, where the growing season is short, seasonal cold temperatures primarily limit productivity (Figure 3).

In the Amazon forest, western and central United States, southern Australia, and Africa, GPP limitation is more related to water constraints (VPD and SM) through the negative impact of high VPD and the positive

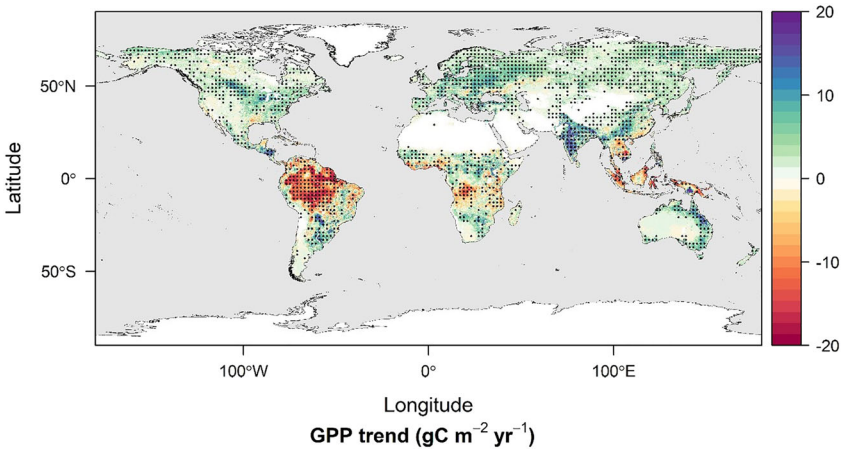

Figure 1. Trends in global gross primary productivity (GPP) for 1982–2016.

impact of SM availability. In tropical rainforest, GPP is controlled by the amount of incoming radiation and the negative impact of high VPD (Figure 3).

We analyzed the relationships between GPP anomalies at decadal time scales and underlying environmental factors affecting plant activity by detrending the long-term annual data. During the 1980s, global GPP was most strongly correlated with PAR and FPAR, indicating that the water and temperature constraints had a relatively smaller influence on interannual variability in GPP (Figure 4). Since in the LUE model the cold temperature constraint factor controls the length of the growing season, it exerts the strongest control in seasonally cold environments such as temperate forests and northern high-latitude ecosystems. On the other hand, the sensitivity of productivity to SM, which has a stronger influence on the productivity in arid environments, has not significantly changed in 2000s compared to previous decades. However, with increasing temperature, the cold temperature constraint effect declines, while correlations with VPD, which limits the productivity during the growing season, increased after the 1980s, indicating that global GPP is shifting from being temperature limited to VPD limited (Figures 4 and S4).

Because GPP reductions occur primarily in tropical zones (Figure 2), we performed an anomaly analysis for GPP in the tropics. Horizon plots (Figure 5) show how annual GPP in each tropical region has changed relative to the average of annual GPP for 1982–2016. GPP significantly declined after the early 2000s in the Amazon and, to a lesser degree, in Africa, whereas GPP in the Asian rainforests began to decline almost a decade earlier than on other continents. GPP in the Amazon has been declining since the 2005 drought, so its mean annual GPP was ~0.13 Pg C lower during the 2000s (compared to the 35-year average) and has continued to drop by up to −1.2 Pg C year^{-1} after the 2010 drought. The annual average GPP of the African tropics was 8.14 Pg C for the study period; it began to slightly decline after 2000 by about 0.06 Pg C and increased by about 0.03 Pg C after 2010. In the Asian tropics after the 1990s, average GPP indicates a decline of 0.3–2% per decade (0.03–0.17 Pg C).

To unravel the underlying mechanism driving tropical GPP change, we performed a VPD anomaly analysis that directly influenced our modeled GPP results for the tropics. Figure 5b demonstrates that VPD in the Amazon began to increase in the early 2000s. In the African tropics, VPD increased from the mid-1990s to mid-2000s, resulting in decreased GPP compared to the 1982–2016 average. In the Asian tropics, where interannual VPD variability is much lower than in Africa and the Amazon, PAR is a larger limiting factor than VPD (Figure 3).

The correlations between interannual GPP variability and environmental factors that constrain our LUE model in the tropics indicate that, in the Amazon, GPP variability is significantly ($p < 0.05$) correlated with variability in VPD ($R^2 = 0.43$) and PAR ($R^2 = 0.47$) but has no significant correlation with FPAR variability over the 35-year record. However, FPAR showed a low but statistically significant correlation ($p < 0.05$) with GPP after 2005 in the Amazon ($R^2 = 0.16$). Over the 35-year period, the African tropics showed a significant correlation with VPD ($R^2 = 0.21$) but not with PAR and FPAR. GPP in the Asian tropics showed a significant

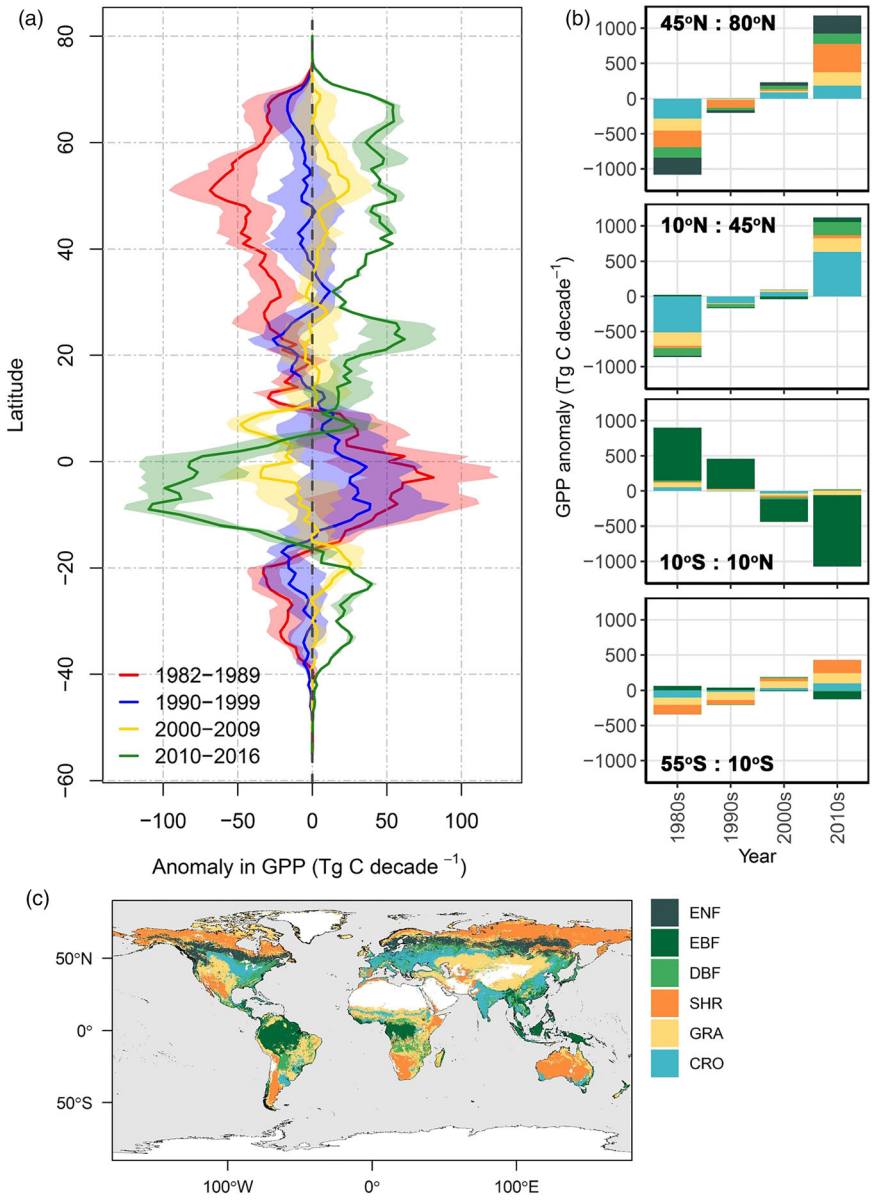

Figure 2. (a) Zonal plot showing global GPP anomalies (departure from mean) binned by latitude and decade. Solid lines and shaded envelopes around each line denote the mean and standard deviation. While GPP steadily increased across the decades in midlatitudes and northern high latitudes, equatorial GPP steadily decreased. (b) Bar plots showing anomalies in annual GPP in Tg C averaged per decade. (c) PFT classification modified from MODIS-MOD12 Type 5 (Friedl et al., 2010) for Evergreen Broadleaf Forests (EBF), Deciduous Broadleaf Forests (DBF), shrub lands (SHR), grasslands (GRA), and croplands (CRO).

correlation with VPD (R^2 = 0.49), a very high correlation with PAR (R^2 = 0.8) and a nonsignificant correlation with FPAR.

We further compared anomalies as a departure from long-term mean values of GPP from the TRENDY models, inversion model CO_2 fluxes, and SIF from the GOME-2 and SCIAMACHY (Figure 6) for tropical and northern northern middle and high latitudes. Our results indicate that, unlike the TRENDY GPP, the GPP_{Enh} model shows a recent variable response of northern ecosystem productivity to climatic changes. GOME-2 SIF also shows a variable annual signal despite focusing on a shorter period compared to GPP_{Enh}, TRENDY, and net biome production (NBP) data from the inversion models. The NBP data show increasing net CO_2 uptake after 2000, even though there is more interannual variation compared to the TRENDY data.

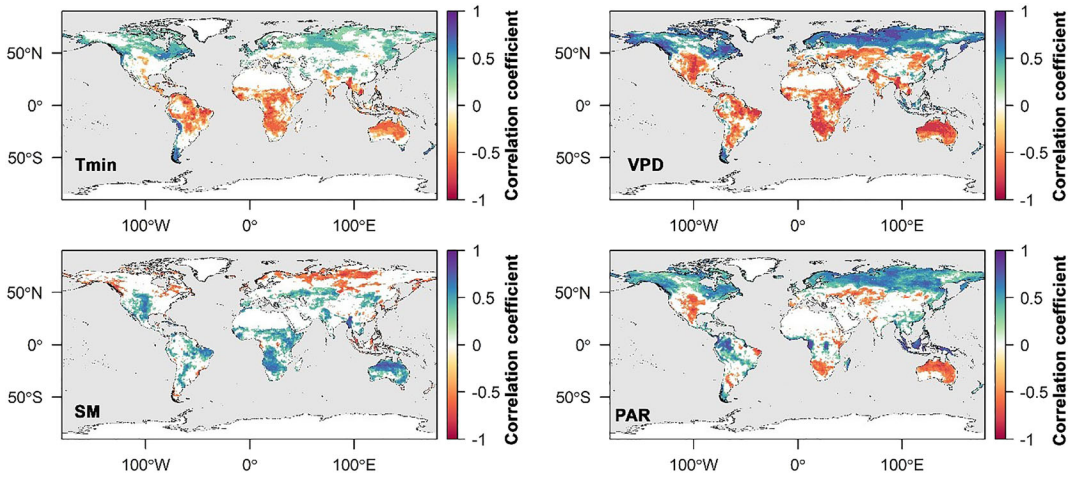

Figure 3. Climatic factors affecting GPP. Dominant environmental constraint factors influencing changes in GPP for the period 1982–2016 derived from the Pearson correlations of minimum daily temperature (T_{min}), vapor pressure deficit (VPD), soil moisture (SM), and photosynthetically active radiation (PAR) to this study's long-term estimated annual GPP. Productivity is primarily related to soil moisture availability and VPD in arid regions and tropics, whereas low temperatures primarily limit productivity in the high northern latitudes. In far northern latitudes and rainforests, ecosystem GPP is positively correlated with the amount of PAR. Nonsignificant correlations are masked out.

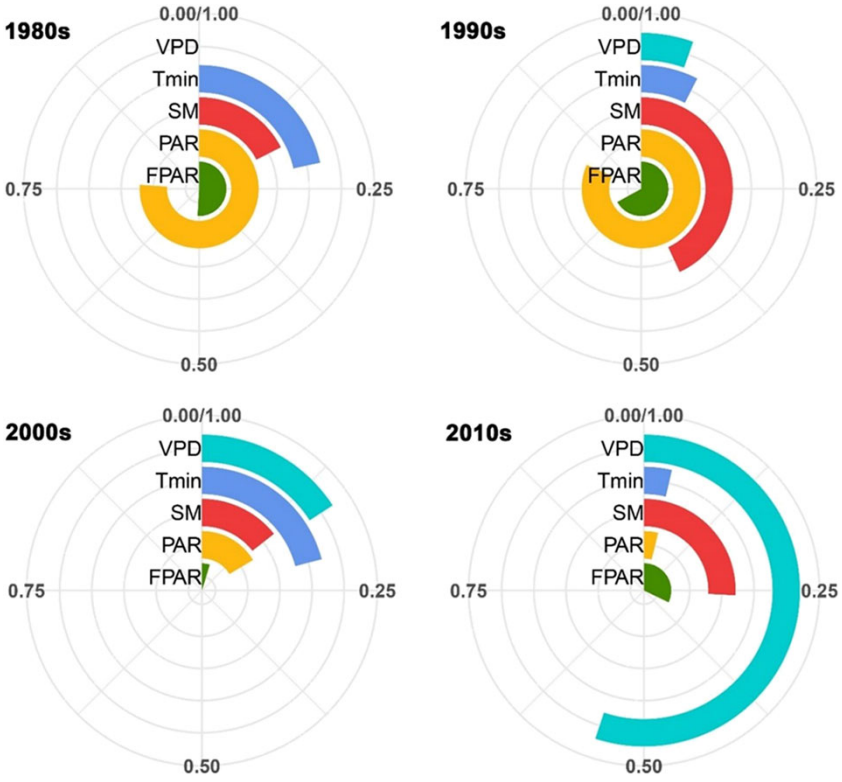

Figure 4. The correlation between interannual GPP anomalies with FPAR, PAR, SM, T_{min}, and VPD. The plot shows the spatial average of such time series correlations in R^2 between anomalies in annual GPP (Pg C year^{-1}) with average detrended FPAR, PAR, SM, T_{min}, and VPD values for the corresponding decade. Interannual GPP before 2000 was highly correlated with FPAR and PAR variations, but global GPP was significantly controlled by higher atmospheric VPD after 2000.

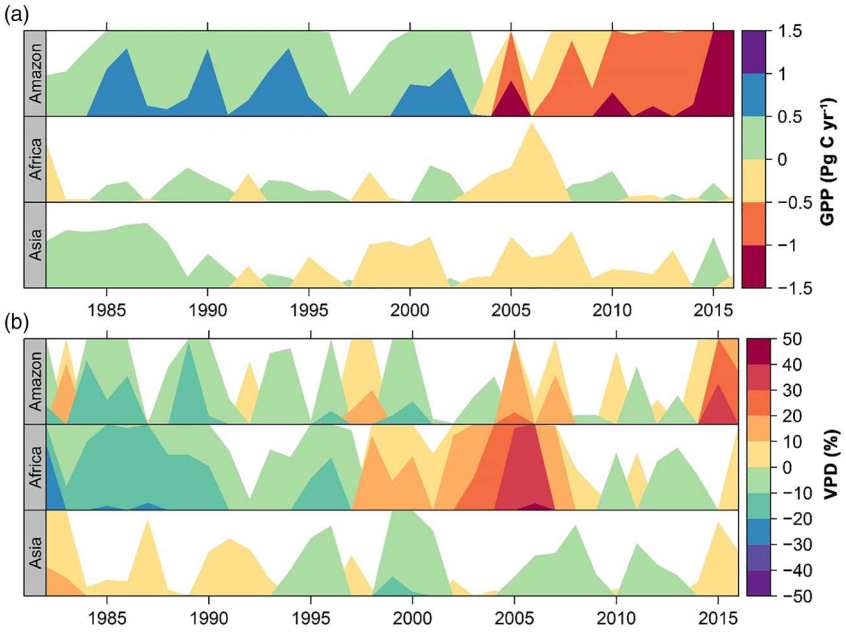

Figure 5. Horizon plot of anomalies in GPP and VPD time series for tropical forests in the Amazon, Africa, and Asia. The plot shows anomalies as departure from (a) average annual GPP (Pg C year^{-1}) and (b) percent change in annual VPD. In the Amazon, GPP anomalies were positive through 2004 and then began to decline thereafter, whereas the GPP of the African forests showed a slight decline in the 2003–2007 period. The Asian tropics showed a declining trend after 1992. Plots divide the data on the *y* axis based on different bands shown in the legend and assign a different color to each band. Negative values are mirrored and values farther from 0 have more intense colors. Bands with higher values are drawn above the bands with lower values.

4. Discussion

Our results indicated increasing trends in annual GPP in middle to high latitudes. The GPP increase shown in the northern tundra and boreal ecosystems (>45°N) supports previous evidence of greening trends observed from long-term satellite records (Myers-Smith et al., 2015; Zhu et al., 2016). Our results also provided evidence of a link to warming and longer growing seasons consistent with recent climate change (Mao et al., 2016; Zhu et al., 2016).

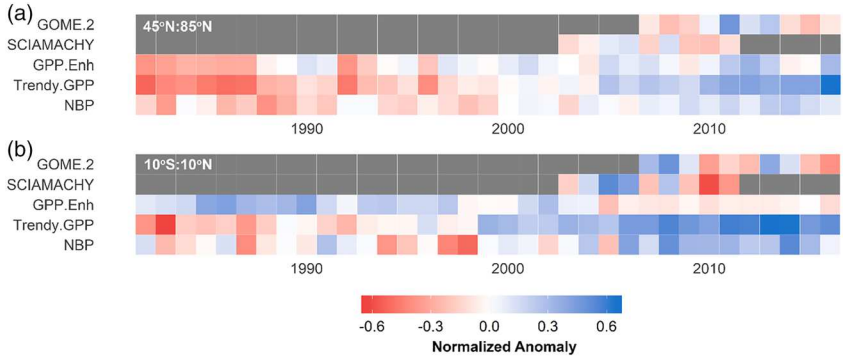

Figure 6. Regional anomalies in long-term ecosystem productivity metrics and estimates. Ecosystem productivity metrics include GOME-2 (2007–2016, Joiner et al., 2012) and SCIAMACHY (2003–2011, Köhler et al., 2015) SIF; GPP models included the enhanced GPP (GPP_{Enh}; this study) and TRENDY GPP (ensemble mean of 10 ecosystem models; Quéré et al., 2018; Sitch et al., 2015), compared with net biome productivity (NBP; ensemble mean from six inversion models, see Table S4 for references) for (a) northern latitudes (> 45°N) and (b) tropical zones (10°S to 10°N). Anomalies as departures from the mean are calculated at regional scales for each year and normalized for visualization and comparisons.

The rapidly changing arctic and boreal ecosystems are crucial components of the Earth system that store more than 30% of terrestrial carbon stocks (Apps et al., 1993; Pan et al., 2011). While boreal ecosystems have remained a persistent terrestrial carbon sink (Ciais et al., 2010), recent models and observations predict that increasing air temperatures will reduce the carbon uptake capacity of these biomes over the next century (Liu et al., 2019; Natali et al., 2019). Longer growing seasons and earlier observed photosynthesis from climate warming (Assmann et al., 2019; Box et al., 2019; Parazoo et al., 2018) lead to increased rate and duration of evapotranspiration which can deplete SM and plant available water in the late growing season (Buermann et al., 2013, 2018; Lian et al., 2019; Parida & Buermann, 2014; Yi et al., 2014; Zhang et al., 2020). Prevalence of warming and browning in the Arctic (Bhatt et al., 2013; Phoenix & Bjerke, 2016; Treharne et al., 2019) also increases the risk of fire occurrences (Hu et al., 2010). All of these factors can affect satellite-observed FPAR and SIF, while our model results also confirm recent high interannual variability in productivity in the northern high latitudes consistent with variability in temperature and water constraints.

Although the GPP increase in the northern high latitudes indicates a persistent, increasing negative carbon-climate feedback, our results suggest an emerging positive feedback to climate in the tropics. The negative GPP trend in the tropics suggests that the increased atmospheric water demand is not balanced by increased available water supply. The changes in rainfall patterns and recent increase in forest mortality in the Amazon forest (Brienen et al., 2015; Phillips et al., 2009; Wigneron et al., 2020) are clear examples of the severe impact of episodic drought and changes in patterns of water supply on these critical ecosystems. These changes in water supply and precipitation forcing in the Amazon influence VPD through land-atmosphere feedback and the trends in PAR.

In contrast to the declining trends seen in GPP_{Enh} in the tropical zones, the TRENDY models show an increase in GPP. LUE models have the advantage over prognostic vegetation models of a direct FPAR observational constraint and can thus potentially reflect anthropogenic effects such as deforestation and human pressure on the tropical hydroclimate system (Khanna et al., 2017) and indirectly impact ecosystem productivity. Like other LUE models, our model is directly constrained by remote sensing observed vegetation indices that have been at the center of debates, especially over dense tropical forests (Bi et al., 2015; Huete et al., 2006; Morton et al., 2014; Saleska et al., 2016). However, our model revealed that there is no significant correlation between interannual variability of GPP in tropical South America with FPAR variability. Instead, we report a strong sensitivity of tropical GPP to VPD variability, which has also been shown for spaceborne SIF (Lee et al., 2013). We analyzed monthly VPD and GPP climatology observed at a CO_2 flux tower site in the Amazon and found a reduction in GPP when VPD increased beyond 800 Pa (Figure S5). Our results are consistent with other reports of increasing VPD at a global scale after the mid-1990s (Yuan et al., 2019) and highlight the potential constraining impact of increasing water limitations on global ecosystem productivity. This is especially true in the tropics, where changes in water constraints can lead to variable responses in net carbon exchange (Liu et al., 2017). However, this VPD impact on productivity seems to be less emphasized in Earth system models (Smith et al., 2016), which show increasing vegetation activity in the tropical zones after 2000 (Figure 7).

In tropical zones, where TRENDY models show increased GPP after 1997, GPP_{Enh} estimates show divergent results, including a reduction in annual GPP after 2004. NBP obtained from inverse models generally indicates enhanced carbon uptake in the tropical zones after 2004 with some variation. It should be noted that inversion models have difficulty modeling the distribution of carbon sources and sinks in the tropics given the intensity of tropical convection, which can affect the spatial distribution of CO_2 concentration (Malhi & Phillips, 2004). In addition, the divergence in productivity estimates between DGVMs and LUE models can be related to DGVM oversensitivity to trends in atmospheric CO_2 fertilization (Smith et al., 2016) including lack of nutrient limitations, as these models tend to have higher sensitivity to CO_2 increase in tropical ecosystems than temperate and boreal ecosystems (Hickler et al., 2008; Schimel et al., 2015). However, it has been argued that most LUE models underestimate the CO_2 fertilization effect, as they do not explicitly account for atmospheric CO_2 concentrations (De Kauwe et al., 2016). LUE models are parametrized using carbon flux towers that have been operational since the late 1990s (Baldocchi et al., 2001). The dynamic effect of CO_2 fertilization on traditional LUE models is only reflected in FPAR observations that show long-term sensitivity to CO_2 trends (Chen et al., 2019; Zhu et al., 2016). Even though we used dynamic

maximum and minimum annual FPAR for LUE_{opt} extrapolation to represent changes in the atmospheric CO_2 growth rate and the effects of land use change on photosynthetic efficiency, it is likely that the long-term trend in our LUE based GPP is underestimated.

As we addressed, our study was limited by the LUE_{opt} estimated for the majority of the flux towers that were operational mostly during the 2000s. However, water and temperature constraints also play a significant role in controlling the growing season length and vegetation phenology. Our results indicate that when climate remained static, the APAR-only model, driven implicitly by leaf area and CO_2 fertilization, increased global GPP for the period 1982–2016 at a rate of 0.1 Pg C $year^{-1}$ (Figure S6). The addition of climate constraints reduces the global APAR-driven GPP trend by 10% to 0.09 Pg C $year^{-1}$. However, it is important to note that the long-term trends here are affected by nonstationarity in time series. For example, large ENSO events affect these trends, but our results indicate that climate warming and drying in the tropics are gradually reducing the GPP growth rate at global scale. This estimated annual GPP trend is significantly lower than the TRENDY estimated GPP trend of 0.57 Pg C $year^{-1}$, which optimistically follows the atmospheric CO_2 growth rate pattern (Figure S7).

Our GPP approach of using spatially and temporally variable LUE_{opt} shows significant improvements over using fixed predefined LUE_{max} values per biome type (Figures S2 and S3). The LUE_{opt} model is based on the concept that ecosystem processes differ based on plant community compositing and that consideration of the geographic location and key life history traits of plants better accounts for the range of plant functional relationships with climate (Madani et al., 2014). Improving the LUE concept should also lead to better understanding of the response of plant productivity to climate change, despite the limitations associated with our LUE model approach as a whole.

Here, we focused only on the uncertainties related to extrapolated LUE (Figure S8) that were caused by random errors. At the global scale, these errors correspond to less than 10% of the LUE values for PFTs (Figure S9) and 6 Pg C standard deviation in annual GPP estimates. The resulting standard deviation around GPP estimates (Figure S10) does not affect our key findings. Nonetheless, uncertainties are involved in each of the LUE model inputs (Zhao et al., 2005) including the MERRA-2 surface meteorological data. Like all reanalysis data, MERRA-2 estimates may be impacted adversely by discontinuities in the assimilated satellite observing system record that impact the modeled water and energy fluxes (Gelaro et al., 2017; Robertson et al., 2016). Moreover, the use of gauge-based precipitation forcing in MERRA-2 can likewise result in discontinuities, especially in poorly observed regions such as the Amazon (Reichle et al., 2017; their Figure 8).

Even though CO_2 fertilization and nutrient effects are indirectly considered in the remote sensing-derived FPAR observations and the spatially explicit estimation of LUE_{opt} model, future work should more directly account for these effects. Further improvement in the LUE models by including higher spatiotemporal resolution meteorological information capturing local variations in SM (due to topography) and incoming shortwave radiation (due to clouds, diffuse and direct fraction), better representation of disturbance events such wildfires, and full representation of plant water availability, such as the inclusion of surface-to-groundwater information and the assimilation of satellite data (Madani et al., 2020; Smith et al., 2019), may further improve the model correspondence with productivity benchmark observations derived from the satellite SIF and global carbon flux tower record. These improvements will enable more accurate assessments and attribution of long-term climate and CO_2 effects and improved benchmarking of DGVMs, giving us better insight into future productivity changes.

Conflict of Interest

The authors declare no conflicts of interest relevant to this study.

Data Availability Statement

The data produced from this study are accessible to the public through the ORNL DAAC (https://doi.org/10.3334/ORNLDAAC/1789) and NTSG publicportal at http://files.ntsg.umt.edu. All data used in this research are publicly available from the cited literature and the following links: MERRA-2 data are available online (https://gmao.gsfc.nasa.gov/reanalysis/MERRA-2/data_access/). GIMMS 3g FPAR data can be

accessed from http://sites.bu.edu/cliveg/ website. SIF data can be accessed from GODDARD Space Flight Center data portal (https://avdc.gsfc.nasa.gov/pub/data/satellite/). TRENDY data can be obtained online (http://dgvm.ceh.ac.uk/node/9/index.html). FLUXNET data are available on ORNL DAAC https://daac.ornl.gov/cgi-bin/dataset_lister.pl?p=9 and at https://fluxnet.org/data/fluxnet2015-dataset/ website. Carbon tracker is obtained from NOAA Earth System Research Laboratory (https://www.esrl.noaa.gov/gmd/ccgg/carbontracker/), Carbon Tracker Europe from Wageningen University (http://www.carbontracker.eu/), Jena CarboScope is from MPG (http://www.bgc-jena.mpg.de/CarboScope/), and CAMS from ECMWF (http://apps.ecmwf.int/datasets/data/cams-ghg-inversions/). MODIS data are available to download online (https://lpdaac.usgs.gov/).

Acknowledgments
This research was funded by the National Aeronautics and Space Administration (NASA) under an IDS project carried out at the Jet Propulsion Laboratory, California Institute of Technology, under a contract with NASA, copyright 2020 California Institute of Technology. T. T. was funded by the Swedish National Space Board (Dnr 95/16). J. S. K. and M. P. M. were funded by USDA NIFA Grant 2016-67026-25067 and NASA EPSCoR 80NSSC18M0025M. R. R. was supported by the NASA Modeling, Analysis, and Prediction Program.

References

Anav, A., Friedlingstein, P., Beer, C., Ciais, P., Harper, A., Jones, C., et al. (2015). Spatiotemporal patterns of terrestrial gross primary production: A review. *Reviews of Geophysics*, *53*, 785–818. https://doi.org/10.1002/2015RG000483

Apps, M. J., Kurz, W. A., Luxmoore, R. J., Nilsson, L. O., Sedjo, R. A., Schmidt, R., et al. (1993). Boreal forests and tundra. *Water, Air, and Soil Pollution*, *70*(1–4), 39–53. https://doi.org/10.1007/BF01104987

Assmann, J. J., Myers-Smith, I. H., Phillimore, A. B., Bjorkman, A. D., Ennos, R. E., Prevéy, J. S., et al. (2019). Local snow melt and temperature—But not regional sea ice—Explain variation in spring phenology in coastal Arctic tundra. *Global Change Biology*, *25*(7), 2258–2274. https://doi.org/10.1111/gcb.14639

Baldocchi, D. (2008). Breathing of the terrestrial biosphere: Lessons learned from a global network of carbon dioxide flux measurement systems. *Australian Journal of Botany*, *56*(1), 1–26. Retrieved from. https://doi.org/10.1071/BT07151

Baldocchi, D., Falge, E., Gu, L., Olson, R., Hollinger, D., Running, S., et al. (2001). FLUXNET: A new tool to study the temporal and spatial variability of ecosystem-scale carbon dioxide, water vapor, and energy flux densities. *Bulletin of the American Meteorological Society*, *82*(11), 2415–2434. https://doi.org/10.1175/1520-0477

Beer, C., Reichstein, M., Tomelleri, E., Ciais, P., Jung, M., Carvalhais, N., et al. (2010). Terrestrial gross carbon dioxide uptake: Global distribution and covariation with climate. *Science*, *329*(5993), 834–838. https://doi.org/10.1126/science.1184984

Bhatt, U. S., Walker, D. A., Raynolds, M. K., Bieniek, P. A., Epstein, H. E., Comiso, J. C., et al. (2013). Recent declines in warming and vegetation greening trends over pan-arctic tundra. *Remote Sensing*, *5*(9), 4229–4254. https://doi.org/10.3390/rs5094229

Bi, J., Knyazikhin, Y., Choi, S., Park, T., Barichivich, J., Ciais, P., et al. (2015). Sunlight mediated seasonality in canopy structure and photosynthetic activity of Amazonian rainforests. *Environmental Research Letters*, *10*(6), 064014. https://doi.org/10.1088/1748-9326/10/6/064014

Box, J. E., Colgan, W. T., Christensen, T. R., Schmidt, N. M., Lund, M., Parmentier, F. J. W., et al. (2019). Key indicators of Arctic climate change: 1971-2017. *Environmental Research Letters*, *14*(4), 045010. https://doi.org/10.1088/1748-9326/aafc1b

Brienen, R. J. W., Phillips, O. L., Feldpausch, T. R., & Al, E. (2015). Long-term decline of the Amazon carbon sink. *Nature*, *519*(7543), 344–348. https://doi.org/10.1038/nature14283

Buermann, W., Bikash, P. R., Jung, M., Burn, D. H., & Reichstein, M. (2013). Earlier springs decrease peak summer productivity in North American boreal forests. *Environmental Research Letters*, *8*(2). https://doi.org/10.1088/1748-9326/8/2/024027

Buermann, W., Forkel, M., O'Sullivan, M., & Richardson, A. (2018). Widespread seasonal compensation effects of spring warming on plant productivity in northern ecosystems. *Nature*, *562*(7725), 110–114. https://doi.org/10.1038/s41586-018-0555-7

Chen, J. M., Ju, W., Lu, X., & Ciais, P. (2019). Vegetation structural change since 1981 significantly enhanced the terrestrial carbon sink. *Nature Communications*, *10*(1), 1–7. https://doi.org/10.1038/s41467-019-12257-8

Ciais, P., Canadell, J. G., Luyssaert, S., Chevallier, F., Shvidenko, A., Poussi, Z., et al. (2010). Can we reconcile atmospheric estimates of the Northern terrestrial carbon sink with land-based accounting? *Current Opinion in Environmental Sustainability*, *2*(4), 225–230. https://doi.org/10.1016/j.cosust.2010.06.008

Cleland, E. E., Chuine, I., Menzel, A., Mooney, H. A., & Schwartz, M. D. (2007). Shifting plant phenology in response to global change. *Trends in Ecology & Evolution*, *22*(7), 357–365. https://doi.org/10.1016/j.tree.2007.04.003

Cong, N., Wang, T., Nan, H., Ma, Y., Wang, X., Myneni, R. B., & Piao, S. (2013). Changes in satellite-derived spring vegetation green-up date and its linkage to climate in China from 1982 to 2010: A multimethod analysis. *Global Change Biology*, *19*(3), 881–891. https://doi.org/10.1111/gcb.12077

De Kauwe, M. G., Keenan, T. F., Medlyn, B. E., Prentice, I. C., & Terrer, C. (2016). Satellite based estimates underestimate the effect of CO_2 fertilization on net primary productivity. *Nature Climate Change*, *6*(10), 892–893. https://doi.org/10.1038/nclimate3105

Etheridge, D. M., Steele, L. P., Langenfelds, R. L., Francey, R. J., Barnola, J. M., & Morgan, V. I. (1996). Natural and anthropogenic changes in atmospheric CO_2 over the last 1000 years from air in Antarctic ice and firn. *Journal of Geophysical Research*, *101*(D2), 4115–4128. https://doi.org/10.1029/95JD03410

Friedl, M. A., Sulla-Menashe, D., Tan, B., Schneider, A., Ramankutty, N., Sibley, A., & Huang, X. (2010). MODIS collection 5 global land cover: Algorithm refinements and characterization of new datasets. *Remote Sensing of Environment*, *114*(1), 168–182. https://doi.org/10.1016/j.rse.2009.08.016

Gelaro, R., McCarty, W., Suárez, M. J., Todling, R., Molod, A., Takacs, L., et al. (2017). The modern-era retrospective analysis for research and applications, version 2 (MERRA-2). *Journal of Climate*, *30*(14), 5419–5454. https://doi.org/10.1175/JCLI-D-16-0758.1

Hastie, T. J., & Tibshirani, R. (1990). Generalized additive models. *Statistical Science*. https://doi.org/10.1016/j.csda.2010.05.004

Hickler, T., Smith, B., Prentice, I. C., Mjöfors, K., Miller, P., Arneth, A., & Sykes, M. T. (2008). CO_2 fertilization in temperate FACE experiments not representative of boreal and tropical forests. *Global Change Biology*, *14*(7), 1531–1542. https://doi.org/10.1111/j.1365-2486.2008.01598.x

Hu, F. S., Higuera, P. E., Walsh, J. E., Chapman, W. L., Duffy, P. A., Brubaker, L. B., & Chipman, M. L. (2010). Tundra burning in Alaska: Linkages to climatic change and sea ice retreat. *Journal of Geophysical Research*, *115*, G04002. https://doi.org/10.1029/2009JG001270

Huete, A. R., Didan, K., Shimabukuro, Y. E., Ratana, P., Saleska, S. R., Hutyra, L. R., et al. (2006). Amazon rainforests green-up with sunlight in dry season. *Geophysical Research Letters*, *33*, L06405. https://doi.org/10.1029/2005GL025583

Joiner, J., Yoshida, Y., Vasilkov, A. P., Middleton, E. M., Campbell, P. K. E., Yoshida, Y., et al. (2012). Filling-in of near-infrared solar lines by terrestrial fluorescence and other geophysical effects: Simulations and space-based observations from SCIAMACHY and GOSAT. *Atmospheric Measurement Techniques*, *5*(4), 809–829. https://doi.org/10.5194/amt-5-809-2012

Jones, L. A., Kimball, J. S., Reichle, R. H., Madani, N., Glassy, J., Ardizzone, J. V., et al. (2017). The SMAP level 4 carbon product for monitoring ecosystem land-atmosphere CO_2 exchange. *IEEE Transactions in Geoscience and Remote Sensing*, *55*(11), 6517–6532. https://doi.org/10.1109/TGRS.2017.2729343

Keeling, C. D., Piper, S. C., Bacastow, R. B., Wahlen, M., Whorf, T. P., Heimann, M., & Meijer, H. A. (2005). Atmospheric CO_2 and $^{13}CO_2$ exchange with the terrestrial biosphere and oceans from 1978 to 2000: Observations and carbon cycle implications BT—A history of atmospheric CO_2 and its effects on plants. *Animals, and Ecosystems*, 83–113. https://doi.org/10.1007/0-387-27048-5_5

Keenan, T. F., Prentice, I. C., Canadell, J. G., Williams, C., Wang, H., Raupach, M. R., & Collatz, G. J. (2016). Recent pause in the growth rate of atmospheric CO_2 due to enhanced terrestrial carbon uptake. *Nature Communications*, 1–9. https://doi.org/10.1038/ncomms13428

Kergoat, L., Lafont, S., Arneth, A., Le Dantec, V., & Saugier, B. (2008). Nitrogen controls plant canopy light-use efficiency in temperate and boreal ecosystems. *Journal of Geophysical Research*, *113*, G04017. https://doi.org/10.1029/2007JG000676

Khanna, J., Medvigy, D., Fueglistaler, S., & Walko, R. (2017). Regional dry-season climate changes due to three decades of Amazonian deforestation. *Nature Climate Change*, *7*(3), 200–204. https://doi.org/10.1038/NCLIMATE3226

Kimball, J. S., Jones, L. A., Glassy, J., Madani, N., & Reichle, R. H. (2017). Monitoring ecosystem-atmosphere CO_2 exchange response to recent (2015-2016) climate variability using the smap l4 carbon product. In 2017 IEEE International Geoscience and Remote Sensing Symposium (IGARSS), Fort Worth, TX. (pp. 2557–2560). https://doi.org/10.1109/IGARSS.2017.8127517

Kimball, J. S., Reichle, R., Neill, P. O., Mcdonald, K., & Njoku, E. (2012). Soil moisture active passive (SMAP) algorithm theoretical basis document (ATBD) SMAP level 4 carbon data product. NASA National Snow and Ice Data Center Distributed Active Archive Center.

Köhler, P., Guanter, L., & Joiner, J. (2015). A linear method for the retrieval of sun-induced chlorophyll fluorescence from GOME-2 and SCIAMACHY data. *Atmospheric Measurement Techniques*, *8*(6), 2589–2608. https://doi.org/10.5194/amt-8-2589-2015

Lee, J.-E., Frankenberg, C., van der Tol, C., Berry, J. A., Guanter, L., Boyce, C. K., et al. (2013). Forest productivity and water stress in Amazonia: Observations from GOSAT chlorophyll fluorescence. *Proceedings of the Royal Society B: Biological Sciences*, *280*(1761), 20130171. https://doi.org/10.1098/rspb.2013.0171

Lian, X., Piao, S., Li, L. Z. X., Li, Y., Huntingford, C., Ciais, P., et al. (2019). Summer soil drying exacerbated by earlier spring greening of northern vegetation. *Science Advances*, *6*(1), eaax0255. https://doi.org/10.1126/sciadv.aax0255

Liu, J., Bowman, K. W., Schimel, D. S., Parazoo, N. C., Jiang, Z., Lee, M., et al. (2017). Contrasting carbon cycle responses of the tropical continents to the 2015-2016 El Nino. *Science*, *358*(3660), 1–7. https://doi.org/10.1126/science.aam5690

Liu, Z., Kimball, J. S., Parazoo, N. C., Ballantyne, A. P., Wang, W. J., Madani, N., et al. (2019). Increased high-latitude photosynthetic carbon gain during an anomalously warm spring offset by respiration carbon loss during preceding winter R. *Global Change Biology*, *26*(2), 682–696. https://doi.org/10.1111/gcb.14863

Madani, N., Kimball, J. S., Affleck, D. L. R., Kattge, J., Graham, J., van Bodegom, P. M., et al. (2014). Improving ecosystem productivity modeling through spatially explicit estimation of optimal light use efficiency. *Journal of Geophysical Research: Biogeosciences*, *119*, 1755–1769. https://doi.org/10.1002/2014JG002709

Madani, N., Kimball, J. S., Jones, L. A., Parazoo, N. C., & Guan, K. (2017). Global analysis of bioclimatic controls on ecosystem productivity using satellite observations of solar-induced chlorophyll fluorescence. *Remote Sensing*, *9*(530), 1–16. https://doi.org/10.3390/rs9060530

Madani, N., Kimball, J. S., Parazoo, N. C., Ballantyne, A. P., Tagesson, T., Jones, L. A., et al. (2020). Below-surface water mediates the response of African forests to reduced rainfall. *Environmental Research Letters*, *15*(3), 034063. https://doi.org/10.1088/1748-9326/ab724a

Madani, N., Kimball, J. S., & Running, S. W. (2017). Improving global gross primary productivity estimates by computing optimum light use efficiencies using flux tower data. *Journal of Geophysical Research: Biogeosciences*, *122*, 2939–2951. https://doi.org/10.1002/2017JG004142

Malhi, Y., & Phillips, O. L. (2004). Tropical forests and global atmospheric change—Introduction. *Philosophical Transactions Of The Royal Society Of London Series B-Biological Sciences*, *359*(1443), 309–310.

Mao, J., Ribes, A., Yan, B., Shi, X., Thornton, P. E., Séférian, R., et al. (2016). Human-induced greening of the northern extratropical land surface. *Nature Climate Change*, *6*(10), 959–963. https://doi.org/10.1038/NCLIMATE3056

Morton, D. C., Nagol, J., Carabajal, C. C., Rosette, J., Palace, M., Cook, B. D., et al. (2014). Amazon forests maintain consistent canopy structure and greenness during the dry season. *Nature*, *506*(7487), 221–224. https://doi.org/10.1038/nature13006

Murray, F. W. (1967). On the computation of saturation vapor pressure. *Journal of Applied Meteorology*. https://doi.org/10.1175/1520-0450(1967)006<0203:OTCOSV>2.0.CO;2

Myers-Smith, I. H., Elmendorf, S. C., Beck, P. S. A., Wilmking, M., Hallinger, M., Blok, D., et al. (2015). Climate sensitivity of shrub growth across the tundra biome. *Nature Climate Change*, *5*, 887–891. https://doi.org/10.1038/nclimate2697

Myneni, R. B., Hoffman, S., Knyazikhin, Y., Privette, J. L., Glassy, J., Tian, Y., et al. (2002). Global products of vegetation leaf area and fraction absorbed PAR from year one of MODIS data. *Remote Sensing of Environment*, *83*(1–2), 214–231. ISSN 0034-4257. https://doi.org/10.1016/S0034-4257(02)00074-3

Natali, S. M., Watts, J. D., Rogers, B. M., Potter, S., Ludwig, S. M., Selbmann, A. K., et al. (2019). Large loss of CO_2 in winter observed across the northern permafrost region. *Nature Climate Change*, *9*(11), 852–857. https://doi.org/10.1038/s41558-019-0592-8

Nemani, R. R., Keeling, C. D., Hashimoto, H., Jolly, W. M., Piper, S. C., Tucker, C. J., et al. (2003). Climate-driven increases in global terrestrial net primary production from 1982 to 1999. *Science (New York, N.Y.)*, *300*(5625), 1560–1563. https://doi.org/10.1126/science.1082750

Norby, R. J., Warren, J. M., Iversen, C. M., Medlyn, B. E., & McMurtrie, R. E. (2010). CO_2 enhancement of forest productivity constrained by limited nitrogen availability. *Proceedings of the National Academy of Sciences of the United States of America*, *107*(45), 19,368–19,373. https://doi.org/10.1073/pnas.1006463107

Pan, Y., Birdsey, R. A., Fang, J., Houghton, R., Kauppi, P. E., Kurz, W. A., et al. (2011). A large and persistent carbon sink in the world's forests. *Science*, *333*(6045), 988–993. https://doi.org/10.1126/science.1201609

Parazoo, N. C., Arneth, A., Pugh, T. A. M., Smith, B., Steiner, N., Luus, K., et al. (2018). Spring photosynthetic onset and net CO_2 uptake in Alaska triggered by landscape thawing. *Global Change Biology*, *24*(8), 3416–3435. https://doi.org/10.1111/gcb.14283

Parida, B., & Buermann, W. (2014). Increasing summer drying in North American ecosystems in response to longer nonfrozen periods. *Geophysical Research Letters*, *41*, 5476–5483. https://doi.org/10.1002/2014GL060495

Pastorello, G., Trotta, C., Canfora, E., Chu, H., Christianson, D., Cheah, Y.-W., et al. (2020). The FLUXNET2015 dataset and the ONEFlux processing pipeline for eddy covariance data. *Scientific Data*, *7*(1), 225. https://doi.org/10.1038/s41597-020-0534-3

Phillips, O. L., Aragão, L. E. O. C. L., Lewis, S. L. S. S. L. S., Fisher, J. B. J., Lloyd, J., López-González, G., et al. (2009). Drought sensitivity of the Amazon rainforest. *Science (New York, N.Y.)*, *323*(5919), 1344–1347. https://doi.org/10.1126/science.1164033

Phoenix, G. K., & Bjerke, J. W. (2016). Arctic browning: Extreme events and trends reversing arctic greening. *Global Change Biology*. https://doi.org/10.1111/gcb.13261

Quéré, C., Andrew, R., Friedlingstein, P., Sitch, S., Hauck, J., Pongratz, J., et al. (2018). Global carbon budget 2018. *Earth System Science Data*, *10*(4), 2141–2194. https://doi.org/10.5194/essd-10-2141-2018

Reichle, R. H., Liu, Q., Koster, R. D., Draper, C. S., Mahanama, S. P. P., & Partyka, G. S. (2017). Land surface precipitation in MERRA-2. *Journal of Climate*, *30*(5), 1643–1664. https://doi.org/10.1175/JCLI-D-16-0570.1

Reichstein, M., Bahn, M., Ciais, P., Frank, D., Mahecha, M. D., Seneviratne, S. I., et al. (2013). Climate extremes and the carbon cycle. *Nature*, *500*(7462), 287–295. https://doi.org/10.1038/nature12350

Robertson, F. R., Bosilovich, M. G., & Roberts, J. B. (2016). Reconciling land-ocean moisture transport variability in reanalyses with P—ET in observationally driven land surface models. *Journal of Climate*, *29*(23), 8625–8646. https://doi.org/10.1175/JCLI-D-16-0379.1

Robinson, N. P., Allred, B. W., Smith, W. K., Jones, M. O., Moreno, A., Erickson, T. A., et al. (2018). Terrestrial primary production for the conterminous United States derived from Landsat 30 m and MODIS 250 m. *Remote Sensing in Ecology and Conservation*, *4*(3), 264–280. https://doi.org/10.1002/rse2.74

Running, S. W., Nemani, R. R., Heinsch, F. A., Zhao, M., Reeves, M., & Hashimoto, H. (2004). A continuous satellite-derived measure of global terrestrial primary production. *Bioscience*, *54*(6), 547. https://doi.org/10.1641/0006-3568(2004)054[0547:ACSMOG]2.0.CO;2

Saleska, S. R., Wu, J., Guan, K., Araújo, A., Huete, A. R., & Restrepo-Coupe, N. (2016). Dry-season greening of Amazon forests evidence from ecological studies. *Nature*, *531*(7594), 221–224. https://doi.org/10.1038/nature13006

Schimel, D., Stephens, B. B., & Fisher, J. B. (2015). Effect of increasing CO_2 on the terrestrial carbon cycle. *Proceedings of the National Academy of Sciences*, *112*(2), 436–441. https://doi.org/10.1073/pnas.1407302112

Sitch, S., Friedlingstein, P., Gruber, N., Jones, S. D., Murray-Tortarolo, G., Ahlström, A., et al. (2015). Recent trends and drivers of regional sources and sinks of carbon dioxide. *Biogeosciences*, *12*(3), 653–679. https://doi.org/10.5194/bg-12-653-2015

Smith, W. K., Reed, S. C., Cleveland, C. C., Ballantyne, A. P., Anderegg, W. R. L., Wieder, W. R., et al. (2016). Large divergence of satellite and Earth system model estimates of global terrestrial CO_2 fertilization. *Nature Climate Change*, *6*(3), 306–310. https://doi.org/10.1038/nclimate2879

Smith, W. K., Fox, A. M., MacBean, N., Moore, D. J. P., & Parazoo, N. C. (2019). Constraining estimates of terrestrial carbon uptake: New opportunities using long-term satellite observations and data assimilation. *New Phytologist*. https://doi.org/10.1111/nph.16055

Stocker, B. D., Zscheischler, J., Keenan, T. F., Prentice, I. C., Peñuelas, J., & Seneviratne, S. I. (2018). Quantifying soil moisture impacts on light use efficiency across biomes. *New Phytologist*, *218*(4), 1430–1449. https://doi.org/10.1111/nph.15123

Stocker, B. D., Zscheischler, J., Keenan, T. F., Prentice, I. C., Seneviratne, S. I., & Peñuelas, J. (2019). Drought impacts on terrestrial primary production underestimated by satellite monitoring. *Nature Geoscience*, *12*, 264–270. https://doi.org/10.1038/s41561-019-0318-6

Treharne, R., Bjerke, J. W., Tømmervik, H., Stendardi, L., & Phoenix, G. K. (2019). Arctic browning: Impacts of extreme climatic events on heathland ecosystem CO2 fluxes. *Global Change Biology*, *25*(2), 489–503. https://doi.org/10.1111/gcb.14500

Turner, D. P., Gower, S. T., Cohen, W. B., Gregory, M., & Maiersperger, T. K. (2002). Effects of spatial variability in light use efficiency on satellite-based NPP monitoring. *Remote Sensing of Environment*, *80*(3), 397–405. https://doi.org/10.1016/S0034-4257(01)00319-4

Wang, H., Jia, G., Fu, C., Feng, J., Zhao, T., & Ma, Z. (2010). Deriving maximal light use efficiency from coordinated flux measurements and satellite data for regional gross primary production modeling. *Remote Sensing of Environment*, *114*(10), 2248–2258. https://doi.org/10.1016/j.rse.2010.05.001

Way, J., Ritts, W. D., Cohen, W. B., Maeirsperger, T. K., Gower, S. T., Kirschbaum, A. A., et al. (2005). Site-level evaluation of satellite-based global terrestrial gross primary production and net primary production monitoring. *Global Change Biology*, *11*(4), 666–684. https://doi.org/10.1111/j.1365-2486.2005.00936.x

Wigneron, J. P., Fan, L., Ciais, P., Bastos, A., Brandt, M., Chave, J., et al. (2020). Tropical forests did not recover from the strong 2015–2016 El Niño event. *Science Advances*, *6*(6), 1, eaay4603–11. https://doi.org/10.1126/sciadv.aay4603

Yi, Y., Kimball, J. S., & Reichle, R. H. (2014). Spring hydrology determines summer net carbon uptake in northern ecosystems. *Environmental Research Letters*, *9*(6). https://doi.org/10.1088/1748-9326/9/6/064003

Yuan, W., Zheng, Y., Piao, S., Ciais, P., & Lombardozzi, D. (2019). Increased atmospheric vapor pressure deficit reduces global vegetation growth. *Science Advances*, 1–14.

Zhang, Y., Joiner, J., Gentine, P., & Zhou, S. (2018). Reduced solar-induced chlorophyll fluorescence from GOME-2 during Amazon drought caused by dataset artifacts. *Global Change Biology*, 2229–2230. https://doi.org/10.1111/gcb.14134

Zhang, Y., Parazoo, N. C., Williams, A. P., Zhou, S., & Gentine, P. (2020). Large and projected strengthening moisture limitation on end-of-season photosynthesis. *Proceedings of the National Academy of Sciences*, 201914436. https://doi.org/10.1073/pnas.1914436117

Zhao, M., Heinsch, F. A., Nemani, R. R., & Running, S. W. (2005). Improvements of the MODIS terrestrial gross and net primary production global data set. *Remote Sensing of Environment*, *95*(2), 164–176. https://doi.org/10.1016/j.rse.2004.12.011

Zhao, M., & Running, S. W. (2010). Drought-induced reduction in global terrestrial net primary production from 2000 through 2009. *Science*, *329*(5994), 940–943. https://doi.org/10.1126/science.1192666

Zhu, J., Zhang, M., Zhang, Y., Zeng, X., & Xiao, X. (2018). Response of tropical terrestrial gross primary production to the super El Niño event in 2015. *Journal of Geophysical Research: Biogeosciences*, *123*, 3193–3203. https://doi.org/10.1029/2018JG004571

Zhu, Z., Bi, J., Pan, Y., Ganguly, S., Anav, A., Xu, L., et al. (2013). Global data sets of vegetation leaf area index (LAI)3g and fraction of photosynthetically active radiation (FPAR)3g derived from global inventory modeling and mapping studies (GIMMS) normalized difference vegetation index (NDVI3G) for the period 1981 to 2. *Remote Sensing*, *5*(2), 927–948. https://doi.org/10.3390/rs5020927

Zhu, Z., Piao, S., Myneni, R. B., Huang, M., Canadell, J. G., Ciais, P., et al. (2016). Greening of the Earth and its drivers. *Nature Climate Change*, *6*(8), 791–795. https://doi.org/10.1038/nclimate3004

Zscheischler, J., Mahecha, M. D., Harmeling, S., & Reichstein, M. (2013). Detection and attribution of large spatiotemporal extreme events in Earth observation data. *Ecological Informatics*, *15*, 66–73. https://doi.org/10.1016/j.ecoinf.2013.03.004

Zscheischler, J., Mahecha, M. D., von Buttlar, J., Harmeling, S., Jung, M., Rammig, A., et al. (2014). A few extreme events dominate global interannual variability in gross primary production. *Environmental Research Letters*, *9*(3), 035001. https://doi.org/10.1088/1748-9326/9/3/035001